Proposal 20171538

Title
Fundamental understanding of dominating water transport mode in PEFC gas diffusion layers

Abstract
Water management is the major limiting factor in PEFC for further increase of power density of polymer electrolyte fuel cells (PEFC). The dominating water transport mode in the gas diffusion layer (GDL) of PEFCs is unclear. Operando X-ray tomographic microscopy with 1-2 s acquisition time is required to capture the water distribution in the opague GDL structures dynamically and to conclude on the dominating water transport mode.

Proposer / Spokesperson	
Mr. Hong Xu	Allgemeine Energie (ENE), Paul Scherrer Institut hong.xu@psi.ch

Principal investigator	
Dr. Jens Eller	Allgemeine Energie (ENE), Paul Scherrer Institut

Co-Proposer	
Dr. Felix N Buechi	Allgemeine Energie (ENE), Paul Scherrer Institut
Mrs. Minna Bührer	Photon Science (PSD), Paul Scherrer Institut

Experiment Category	
Experiment Type	Normal
Research Area	Catalytic Materials/Surface Science

Experiment Requirements	
Eligible for EU Support	No
Number of Shifts Required	6
Schedule Preferences	Mai or June
Beamline/Station	TOMCAT

Links to related proposals of relevance to the current proposal		
Proposal	Title/Proposer/Infos given by the proposer about the relation	Report
20170876	Title: Water feature detectability in subsecond XTM of gas diffusion layer of PEFC Proposer: Dr. Jens Eller Infos: During this campaign, water feature detectability under different imaging parameters will be quantified and guide the imaging conditions for operando experiments proposed in this proposal.	Available

A Goal of the experiment

The goal of the proposed experiment is to identify the dominating water transport mode in the gas diffusion layer (GDL) of polymer electrolyte fuel cells (PEFCs). After years of different neutron and X-ray imaging studies it remains still unclear, if the produced water is transported dominantly by either capillary pressure [1] or root-like merging of condensation clusters [2,3] mechanism (see Fig. 1). It is of paramount importance to know which process is dominating and should be considered most of all during future material development. Previous with XTM at static PEFC operation conditions were not able reveal the dominating water transport mode so far. Thanks to the development of dynamic PEFC XTM in second scan time regime ([4], see Fig. 2), the verification of it's imaging capabilities (exp. report 20170876) and the development of water cluster classification algorithms ([5], Fig. 3), it will be possible follow the dynamics of water accumulation in the GDL and identify the driving process.

B Background

Hydrogen fed polymer electrolyte fuel cells (PEFC) are expected to play a major role in a future decarbonized energy system [6], in particular in the mobility sector. Water management is the major limiting factor in PEFC for further increasing power density [7]. Inside the PEFC, the water management is complex: on one hand, the membrane needs a certain hydration state in order to ensure sufficient proton conductivity; on the other hand, excessive water leads to blocked gas pathways in the porous structures with increased mass transport losses (see Fig. 4). These flooding effects can dramatically decrease the accessibility of oxygen, resulting in mass transport limitations ([8], so-called flooding) that prevents high current density operation that is necessary for high power automotive applications.

The dynamic operando XTM setup and image processing knowhow of the proposers was recently used to guide PEFC development in collaboration with a major car manufacturer in during industry beam time at TOMCAT in July 2017.

C Experimental method; specific requirements

Synchrotron radiation based X-ray tomographic microscopy is required due to the fine and opaque fiber structure of the GDL (~7 um fiber diameter) and the transient water transport processes in PEFCs. The fuel cell set-up for operando XTM (see Fig. 5) was developed and exploited during previous campaigns (20090986, 20100287, 20100818, 20110297, 20120161) will be used. It allows precise control of fuel cell operation conditions, eg. in-let gas humidity and cell temperature.

XTM scans with 13.5 keV monochromatic beam energy with voxel size of 3 μm and scan times around 1-2 s is needed to capture of the dynamics of liquid water during operando XTM experiments with a detectability of small water features (>95% detectability for most of the water droplets above diameter of 15 um, see exp. report 20170876). Upcoming microscope upgrade is expected to increase detectability and

to reduce scan time, and thereby dose to the cell per scan, further. XTM scans will be acquired during fuel cell operation at different temperature (30^{o}C, 60^{o}C), low and high current density (0.5A/cm^{2}, 1.0A/cm^{2}) and in-let gas relative humidity varying from 0% (dry gas) to 110% (oversaturated gas) in order to screen for the different water transport modes. Two GDL samples with different pore structures from two different manufacturers (SGL, Toray) will be examined.

D Results expected

With an XTM image acquisition time between 1 - 2 s and feed gas humidity increasing operation conditions, whether a water cluster built up from the catalyst layer towards the GDL-channel/rib interface (capillary pressure driven flow) or growth and aggregation of various independent condensation spots favorable in the GDL domain under the rib (root-like condensation clusters merging), will be clarified. GDL samples from two different manufacturers (SGL, Toray) will be depicted to better understand the influence of the underlying pore structure over a wide range of PEFC operation conditions. These insights into the fundamental water transport mode will potentially guide fuel cell design and material modifications to foster the dominating water transport regime.

E Estimate and justification of the beamtime

Sequences imaging of fuel cells with 2 different GDL samples (SGL, Toray) operating at 2 temperature levels (60^{o}C, 80^{o}C) and 2 current densities (0.5A/cm^{2}, 1.0A/cm^{2}) with increasing gas relative humidity from 0 to 110% will be acquired for 8 cells (2 materials, two repetitions). The estimated average test-time for one cell is 10 h in total (incl. mounting, PEFC operation and XTM acquisition at different conditions with intermediate drying of the cell). Together with fuel cell test bench set-up (4 h per campaign) and beamline setup (2 h) for 4 cells tested at 8 different conditions, a total time of 46 h (4 h +2 h + 4 *10 h) is estimated. Therefore, we apply for a total of 6 shifts (48 h).

F References relevant to the experiment description

[1] S. Litster, D. Sinton, N. Djilali, J. Power Sources, 154(1), 95-105 (2006).
[2] J. H. Nam, M. Kaviany, Int. J. Heat & Mass Transfer, 46(24), 4595-4611 (2003).
[3] U. Pasaogullari, C. Y. Wang, J. Electrochem. Soc., 151(3), A399-A406 (2004).
[4] J. Eller, F. Marone, F. N. Büchi, ECS Trans. 69(17), 523–531 (2015).
[5] J. Eller, J. Roth, F. Marone, M. Stampanoni, F.N. Buechi, J. Electrochem. Soc. 164 (2), F115-F126 (2017).
[6] IEA; Advanced Fuel Cells Implementing Agreement Annual Report (2009).
[7] D. Hayashi, A. Ida, S. Magome, T. Suzuki, S. Yamaguchi, R. Hori, SAE Technical Paper 01-1188 (2017).
[8] J. Eller, T. Rosén, F. Marone, M. Stampanoni, A. Wokaun, F. N. Büchi, J. Electrochemical Society, 158 (8), B963-B970 (2011).

SLS related publications of the proposers (within the last 18 months)
[1] K. B. Hatzell, J. Eller, S. L. Morelly, M. H. Tang, N. J. Alvarez, Y. Gogotsi; Direct observation of active material interactions in flowable electrodes using X-ray tomography; Faraday Discuss., 199, 511-524 (2017). [2] M. A. Safi, N. I. Prasianakis, J. Mantzaras, A. Lamibrac. F. N. Buechi; Experimental and pore-level numerical investigation of water evaporation in gas diffusion layers of polymer electrolyte fuel cells; Int. J. Heat. Mass Transfer, 115 (A), P238-P249 (2017). [3] J. Eller, J. Roth, F. Marone, M. Stampanoni, F.N. Buechi; Operando properties of gas diffusion layers: Saturation and liquid permeability; J. Electrochem. Soc. 164 (2), F115-F126 (2017). [4] A. Forner-Cuenca, J. Biesdorf, A. Lamibrac, V. Manzi-Orezzoli, F.N. Büchi, L. Gubler, T.J. Schmidt, P. Boillat; Advanced water management in PEFCs: Diffusion layers with patterned wettability: II. Measurement of capillary pressure characteristic with neutron and synchrotron imaging; J. Electrochem. Soc. 163 (9), F1038-F1048 (2016). [5] I. V. Zenyuk, A. Lamibrac, J. Eller, D. Y. Parkinson, F. Marone, F. N. Buechi and Adam Z. Weber; Investigating Evaporation in Gas Diffusion Layers for Fuel Cells with X-ray Computed Tomography; J. Phys. Chem. C, 120 (50), F28701–F28711 (2016). [6] T. Agaesse, A. Lamibrac, F. N. Buechi, J. Pauchet, M. Prat; Validation of pore network simulations of ex-situ water distributions in a gas diffusion layer of proton exchange membrane fuel cells with X-ray tomographic images; J. Power Sources, 331, F462-F474 (2016). [7] A. Lamibrac, J. Roth, M. Toulec, F. Marone, M. Stampanoni and F. N. Buechi; Characterization of Liquid Water Saturation in Gas Diffusion Layers by X-Ray Tomographic Microscopy; J. Electrochem. Soc. 163(3), F202-F209 (2016). [8] S. H. Eberhardt, F. Marone, M. Stampanoni, F. N. Buechi and T. J. Schmidt; Operando Xray Tomographic Microscopy Imaging of HT-PEFC: A Comparative Study of Phosphoric Acid Electrolyte Migration; J. Electrochem. Soc. 163(8), F842-F847 (2016). [9] P. Pietsch, D. Westhoff, J. Feinauer, J. Eller, F. Marone, M. Stampanoni, V. Schmidt and V. Wood; Quantifying microstructural dynamics and electrochemical activity of graphite and silicon-graphite lithium-ion battery anodes; Nature Communications, 7, 12909 (2016).

Other publications of the proposers (within the last 18 months)
[1] M. Suermann, K. Takanohashi, A. Lamibrac, T. J. Schmidt, F. N. Buechi; Influence of Operating Conditions and Material Properties on the Mass Transport Losses of Polymer Electrolyte Water Electrolysis; J. Electrochem. Soc. 164 (9), F973-F980 (2017). [2] M. Suermann, T. Kiupel, T. J. Schmidt, F. N. Buechi; Electrochemical Hydrogen Compression: Efficient Pressurization Concept Derived from an Energetic Evaluation; J. Electrochem. Soc., 164 (12), F1187-F1195 (2017). [3] M. Suermann, A. Patru, T. J. Schmidt, F. N. Buechi; High pressure polymer electrolyte water electrolysis: Test bench development and electrochemical analysis; Int. J. Hydrogen Energy, 42(17), P12076-P12086 (2017). [4] U. Babic, M. Suermann, F. N. Buechi, L. Gubler, T. J. Schmidt; Critical Review—Identifying Critical Gaps for Polymer Electrolyte Water Electrolysis Development; J. Electrochem. Soc. 164 (4), F387-F399 (2017). [5] L. Holzer, O. Pecho, J. Schumacher, Ph. Marmet, O. Stenzel, F.N. Buechi, A. Lamibrac, B. Muench; Microstructure-property relationships in a gas diffusion layer (GDL) for Polymer Electrolyte Fuel Cells, Part I: effect of compression and anisotropy of dry GDL; Electrochimica Acta, 227 F419-434 (2017). [6] M. Suermann, T.J. Schmidt, F.N. Buechi; Cell performance determining parameters in high pressure water electrolysis; Electrochim. Acta, 211, 989-997 (2016). [7] P. Pietsch, M. Hess, W. Ludwig, J. Eller, and V. Wooda; Combining operando synchrotron X-ray tomographic microscopy and scanning X-ray diffraction to study lithium ion batteries; Sci Rep. 6, F27994 (2016).

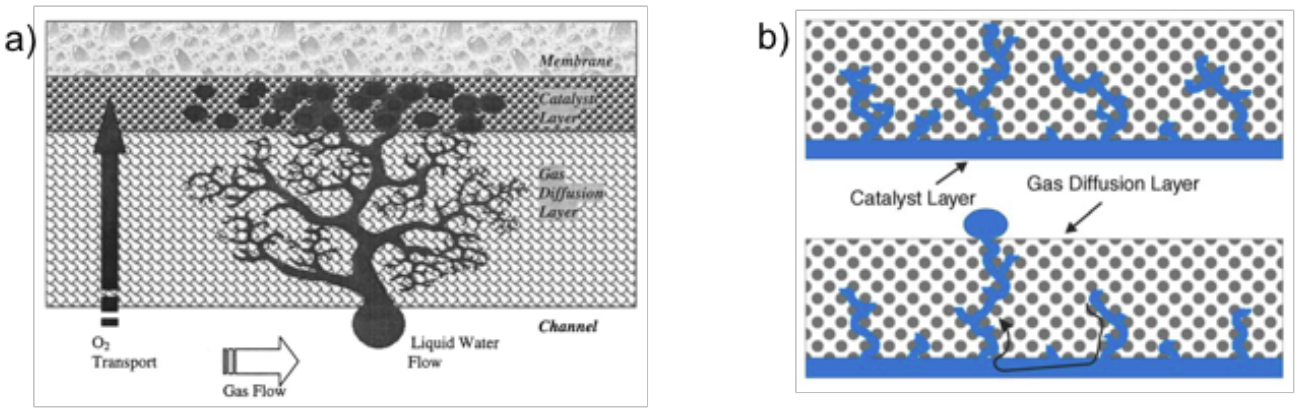

a) Root like merging of condensation clusters.
Nam & Kaviany, Int. J. Heat Mass Trans. ***46*** *(2003)*
Pasaogullari & Wang, J. Elec. Soc. ***151*** *(2004)*

b) Capillary pressure driven liquid flow.
Litster, Sinton, Dijilali, J. Pow. Sources ***154*** *(2006)*

Figure 1: Two fundamental water transport modes in gas diffusion layer (GDL).

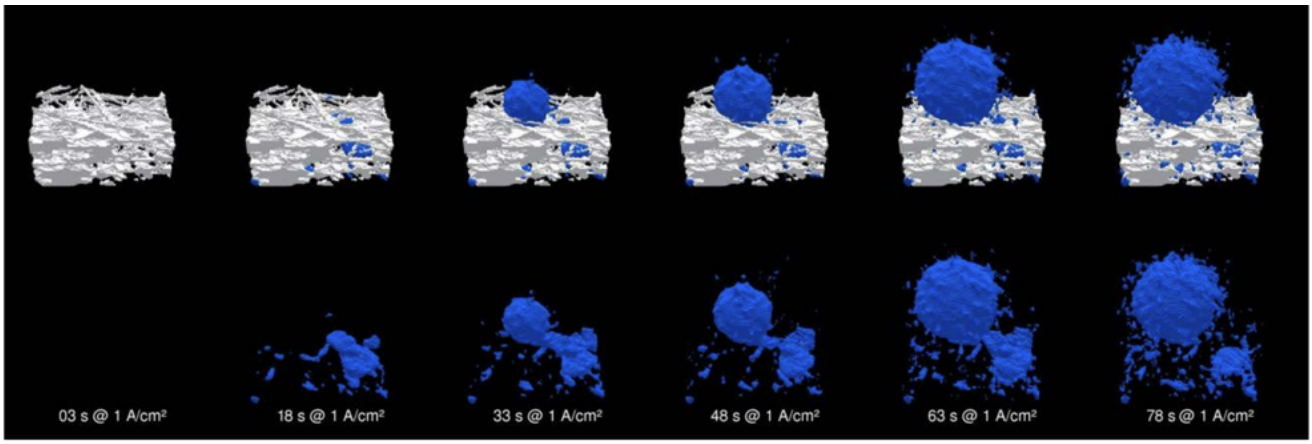

• Surface rendering of the liquid water for selected scans. In the top row, the liquid water is shown together with the solid GDL, while the GDL is not shown in the bottom row; droplet is not removed due to low gas speed (approx. 0.8 m/s).

Figure 2: Subsecond XTM 3D renderings

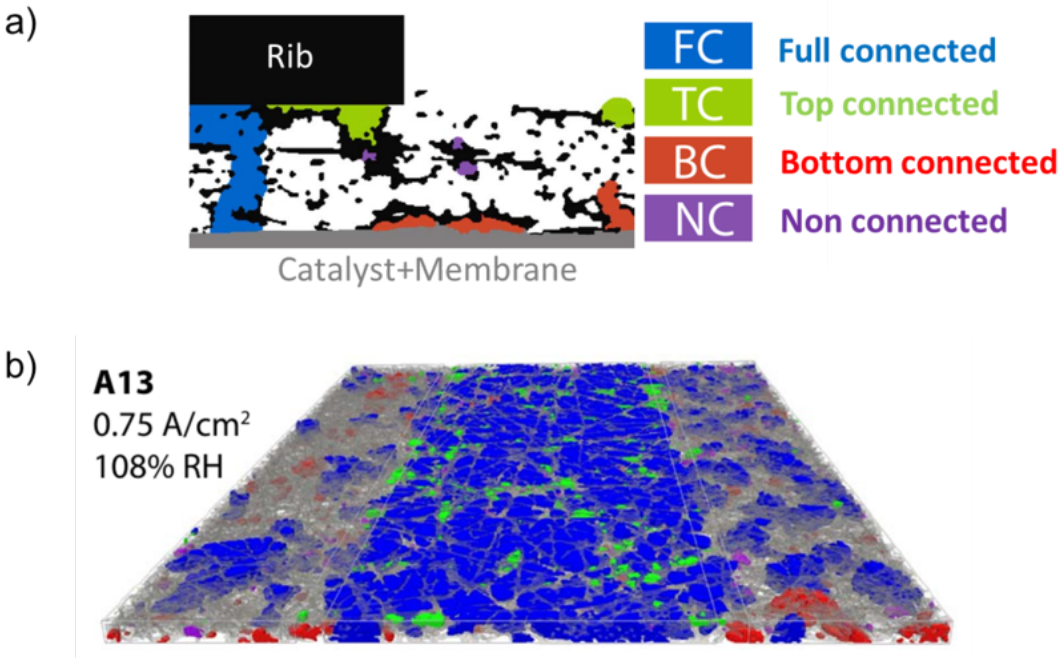

a) Sketch of the different cluster types that can be found in the GDL domain; b) Cluster connectivity analysis of static PEFC scan (scan time 10s)

Figure 3:

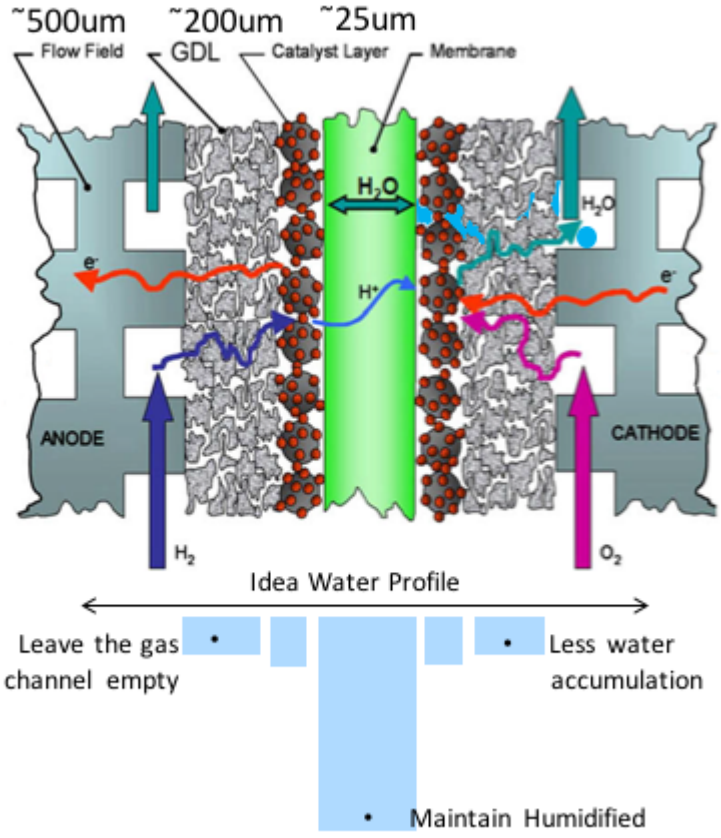

Figure 4: PEFC Scheme and the water profile

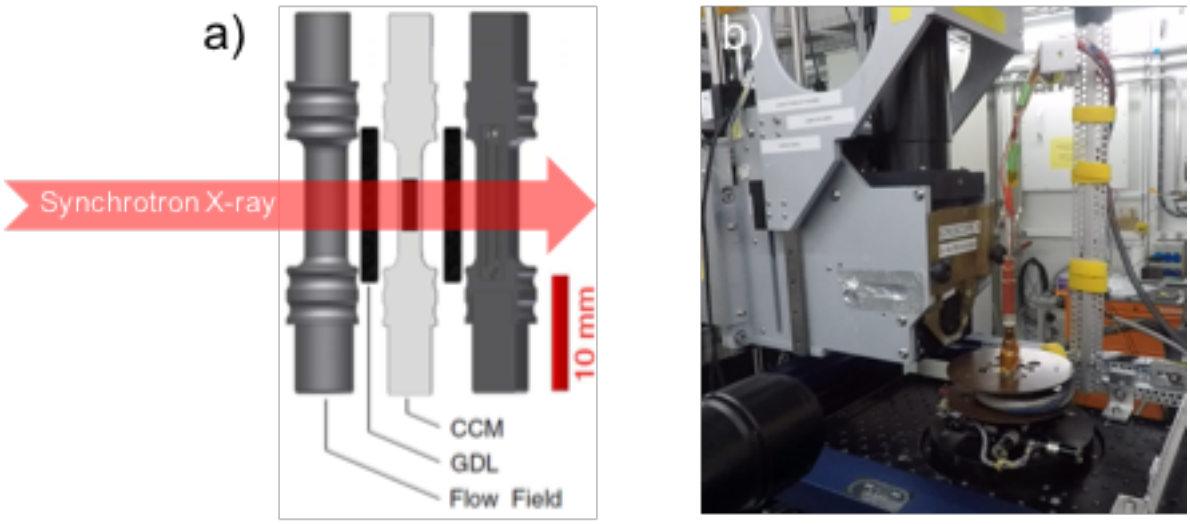

a) Schematic of XTM PEFC components.

b) Operando fuel cell set-up at the beamline in front of the scintillator (X-ray beam coming from the right side).

Figure 5: Image of Setup at beamline

Sample

Sample #1

Sample and chemical substance to be used in this experiment	
Substance	Carbon Fiber; Platinum contained catalyst
Chemical formula	Carbon fiber paper surface-treated with PTFE or FEP; Platnium contained catalyst.
Structure	Multilayer
Size X	5
Size Y	5
Size Z	0.2
Mass	1.6
Container	Vespel cell
High purity	No
After the experiment the sample will be	Removed by user
No ethical issues declared on this sample.	

Sample environment	
Cryojet [K]	270-370
Hotair blower	No
High voltage	No
High pressure	No
High temperature	No
Magnetic field	No
Cryogenic liquid	No
Be window	No

Safety aspects	
Chemical hazards	
Chemical hazards	Burnable chemicals and solvents Gases (CO, H2, N2, O2, CO2, noble gases, others) Reactive chemicals
Specification of chemical hazards	In the setup for running the fuel cell, the sample is overflowed with synthetic air and hydrogen with low gas flow up to 200ml/min
Exhaust disposal conditions	The exhausted gas (air and H2) will be first diluted with N2 and then disposal through TOMCAT exhaust gas pipeline. The disposal gas-diluting set-up has been developed in previous beamtime.

Experimental Report

Water feature detectability in subsecond XTM of gas diffusion layer of PEFC

Hong Xu, Minna Bührer, Jens Eller

(Proposal 20170876)

Overview

The scheduled beamtime on 18th Sept 2017 was dedicated to study the influences by decreasing the XTM scan time towards 0.1 s, which paves the way for 4D XTM imaging of the transient water distribution in the gas diffusion layer (GDL) during polymer electrolyte fuel cell (PEFC) operation. Variations of different imaging parameters (beam energy, scan time) are presented and their consequences on the Contrast-to-Noise (CNR) ratio and further on the detectability of the micro-structural water features are discussed.

Quality of measurement/data

Followed by the proposed experiment in proposal 20170876, XTM scans for a cathode water filled channel fuel cell were collected at four monochromatic beam energy levels (11 keV, 13.5 keV, 16 keV, 18.5 keV) and polychromatic beam energy with variation of scan time from 12.8s to 0.1s. Several high quality scans was taken between the group of scans for the quality checking and comparison. The reconstructed images with missing pixels mask and ring removal were sufficient for post processing and quantification.

Status and progress of evaluation

The data collected at monochromatic beam energy levels are fully reconstructed and processed as presented in the results part. For polychromatic beam data, it is still under optimization of water feature detectability by different reconstruction algorithms. The complete evaluation will be expected to finish before next scheduled beamtime.

Results

In order to improve the image quality towards subsecond X-ray tomographic microscopy, it is vital to understand the influence of imaging conditions on the image quality. The CNR(H_2O/Void) was studied for monochromatic beam energies between 11 keV and 18.5 keV with tomographic scan times ranging from 12.8 s to 0.1 s, which approaches the hardware limitation of image acquisition time 0.05 s at the TOMCAT beamline. The consequences of the time reduction for tomographic scans are shown qualitatively in Figure 1. While the void flow field channels remain visible down to a scan time of 0.1 s in the through-plane slices, the GDL structures can be only seen until 0.8 s scan time in the in-plane view. Some fiber structures are already lost at a scan time of 1.6 s.

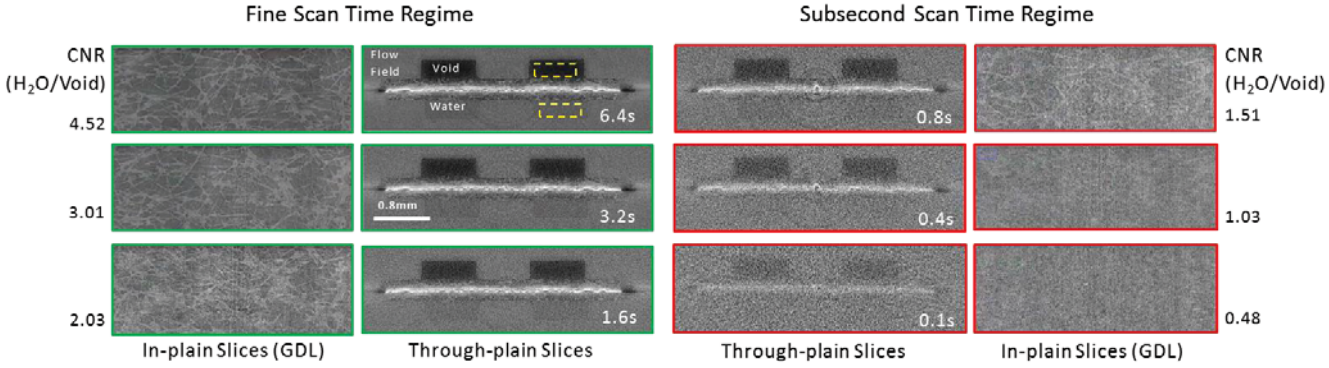

Figure 1: Tomographic in-plain slice and through-plain slice for different tomographic scan times (6.4 s, 3.2 s, 1.6 s, 0.8 s, 0.4 s, 0.1 s) at 13.5 keV; the yellow dashed rectangulars indicate the sampling domains for CNR calculation. The CNR was defined as $\mathrm{CNR}(H_2O/Void) = \frac{mean(H_2O)-mean(Void)}{\sqrt{[StdDev(H_2O)^2+StdDev(Void)^2]/2}}$.

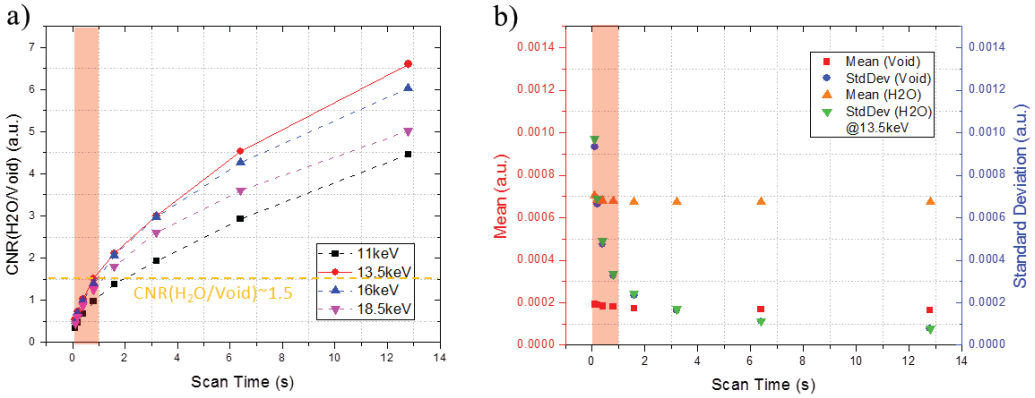

Figure 2: a) Contrast-to-noise ratio between water and void domains for different tomographic scan times at energy levels between 11 keV and 18.5 keV; b) Mean and standard deviation of the H_2O and void domains versus scan time at 13.5 keV; the red area in plot a) and b) indicates the subsecond scan time regime.

At an energy level of 13.5 keV the CNR(H_2O/Void) is the highest for all scan settings (see Figure 2 a). At the lowest energy of 11 keV the X-ray flux and the transmission are lowest and therefore the CNR is smallest for the all scan settings. The reduction of CNR for energies above 13.5 keV is due to the deceasing of the attenuation coefficient of water. For subsecond scan times below 0.8 s the CNR(H_2O/Void) reduces to below 1.5, which challenges the segmentation of the liquid water in the cell. To reveal the reason behind this, a detailed analysis of the contributions of mean and standard deviation levels to the CNR at 13.5 keV is shown in Figure 2 b. The mean gray scale value of both H_2O and void domain remains stable, as the attenuation coefficients are not affected by the scan time. The standard deviations increase as the scan time decreases, especially in the subsecond scan time regime, with similar values for the water and void domains. When the scan time reduces to 0.5 s and below, the standard deviations are almost the same as the mean level of the H_2O domain, and as the noise level reaches the signal level the CNR drops below 1.

The low CNR requires appropriate image denoising before segmentation in order to increase the detection level of the true water domains and to minimize the amount of falsely assigned water domains. Median filter (13) and anisotropic diffusion filter (14) are applied to reduce noise while preserving the edges of the water boundaries. The influence of the number of iterations of the anisotropic diffusion (AD) filter was analyzed for the noise level of 1.6 s scan time. When increasing the number of iterations, the noise in the background decreases (see Figure 3 c). The CNR between water domain and background increases from 2.2 (no AD iteration) to 7.7 (5 AD iterations), which exceeds even the CNR(H_2O/Void) of a 12.8 s scan. This leads to reduction of the falsely segmented water from almost 12 % (no AD iteration) below 1 % (5 AD iterations). The drawback of the strong filtering is a loss of feature detectability which starts already for sphere with a diameter of 10 pixels and cylinder with a diameter of 9 pixels. For larger diameter structures, the anisotropic diffusion filter increases the feature detectability. At cylinder diameters of 5-7 pixels the 5 AD iterations prior to segmentation start to show clearly lower feature detectability levels compared to fewer iterations. This effect becomes more pronounced for even smaller features. 1 pixel diameter cylinders are completely removed by 5 AD iterations, while they can be detected at least partially after 1 AD iteration. Generally, the cylindrical domains show higher feature detectability levels than the spherical domains at the same diameter, as their connectivity is higher (see Figure 3 a-b). 3 AD iterations are identified as a compromise between the detection of small diameter features and the reduction of falsely detected water in the background.

In the following feature detectability analysis, the subtracted image has therefore been filtered with a 3D median filter (radius 1 pixel) and a 3D anisotropic diffusion filter (3 iterations) before segmentation through thresholding. The influence of the scan time on the feature detectability when denoising with 3 AD iterations is presented in Figure 4. A clearly better detection level can be found

for the 3.2 s scan, where feature detectability levels of more than 80 % are observed for cylinders with diameters of 5 pixels and the amount of false water does not exceed 1 %. For the 0.4 s scan, the feature detectability is kept above 60 % with the diameter down to 4 pixels. Due to sampling the virtual water structures only once, fluctuations of feature detectability can be observed for both spherical and cylindrical water clusters with diameter below 8 pixels. Detectability level of subsecond scans needs to be improved. Further studies on threshold level as well as denoising filter combinations are needed. The application of phase retrieval and iterative reconstructions schemes are expected to improve feature detectability further.

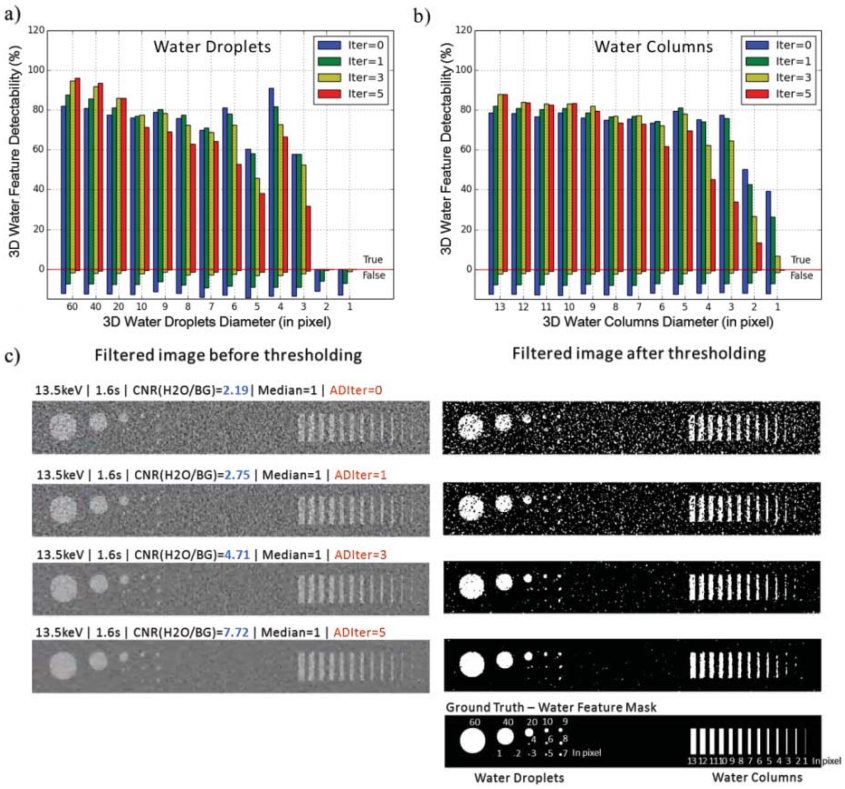

Figure 3: Feature detectability of artificial water droplets a) and water columns b) with various diameters for different number of anisotropic diffusion iterations for a tomographic scan time of 1.6 s at 13.5 keV; bar height above the red line is the percentage of true water voxels in the ground truth domain, bar height below the red line is the percentage of false voxels outside the ground truth within 10 pixels from the surface of the ground truth; c) 2D representation of 3D filtered images and the corresponding segmented images for different number of anisotropic diffusion iterations. The ground truth is shown below as a reference.

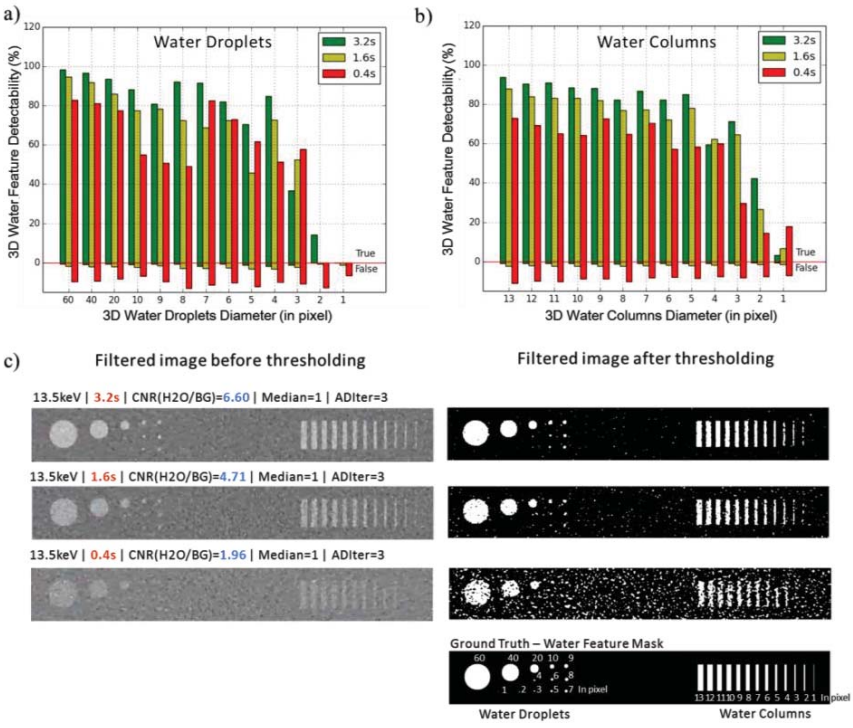

Figure 4: Feature detectability of artificial water droplets a) and water columns b) with different diameters for tomographic scan times 3.2 s, 1.6 s and 0.4 s at 13.5 keV; bar height above the red line is the percentage of true water voxels in the ground truth domain, bar height below the red line is the percentage of false voxels outside the ground truth within 10 pixels from the surface of the ground truth; c) 2D representation of 3D filtered images (left) and the corresponding segmented images (right) for scan times 3.2 s, 1.6 s and 0.4 s. The ground truth is shown below as a reference.

Publications linked to 20170876

Publications linked to this proposal
Fighting the Noise: Towards the Limits of Subsecond X-ray Tomographic Microscopy of PEFC Xu H, Bührer M, Marone F, Schmidt Thomas J, Büchi F, Eller J ECS TRANSACTIONS*80 395 (2017)* DOI : 10.1149/08008.0395ecst

Experimental Report

Fundamental understanding of dominating water transport mode in PEFC gas diffusion layers

Hong Xu, Minna Bührer, Jens Eller

(Proposal 20171538)

Overview

This report will be updated after the scheduled beamtime on 14.06.2018 for proposal 20171538…

Quality of measurement/data

Status and progress of evaluation

Results